Organic Electronics 10 (2009) 27–33

Contents lists available at ScienceDirect

Organic Electronics

journal homepage: www.elsevier.com/locate/orgel

Annealing effect of polymer bulk heterojunction solar cells based on polyfluorene and fullerene blend

Jen-Hsien Huang [a], Chuan-Yi Yang [b], Zhong-Yo Ho [c], Dhananjay Kekuda [d], Meng-Chyi Wu [b], Fan-Ching Chien [d], Peilin Chen [d], Chih-Wei Chu [d,e,*], Kuo-Chuan Ho [a,c,*]

[a] Department of Chemical Engineering , National Taiwan University, Taipei, Taiwan
[b] Institute of Electronic Engineering, National Tsing Hua University, Hsinchu, Taiwan
[c] Institute of Polymer Science and Engineering, National Taiwan University, Taipei, Taiwan
[d] Research Center for Applied Sciences, Academia Sinica, Taipei, Taiwan
[e] Department of Photonics, National Chiao Tung University, Hsinchu, Taiwan

ARTICLE INFO

Article history:
Received 18 July 2008
Received in revised form 19 September 2008
Accepted 20 September 2008
Available online 10 October 2008

PACS:
73.50.Pz
73.61.Ph

Keywords:
Photovoltaic device
Polymer
F8T2
Annealing effect

ABSTRACT

Control of blend morphology at the nanoscale and high charge mobility is essential for polymer photovoltaic devices in terms of their power conversion efficiencies (PCE). In the case of bulk heterojunctions solar cells, both blend morphology and charge mobility are influenced by thermal treatment. In this manuscript, we study the effects of annealing temperature on polymer PV devices with blends of poly[9,9'- dioctyl-fluorene-co-bithiophene] (F8T2) and [6,6]-phenyl-C_{61}-butyric acid methyl ester (PCBM). The morphological changes of blended films were observed upon thermal annealing temperature near and above glass transition temperature (130 °C). Such microstructural transformations resulted in modified charge transport pathways and therefore greately influenced the device performance. The highest PCE of 2.14% with an open-circuit voltage (V_{OC}) of 0.99 V and a short-circuit current (J_{SC}) of 4.24 mA/cm^2 was achieved by device annealing at 70 °C for 20 min.

1. Introduction

Polymer photovoltaic (PV) cells offer great technological potential as a renewable, alternative source of electrical energy including the possibility of low-cost fabrication, low specific weight, and mechanical flexibility. Since solution processed bulk heterojunction (BHJ) solar cells were first reported in mid-1990s, they have been the subject of intense research interests due to their processing advantage as well as the superior mechanical properties of the polymers, such as flexibility. Although the BHJ provides quite a large interface for charge seperation, the power conversion efficiency (PCE) is still limited by the space-charge effects inherent in the BHJ structure due to the imbalance between electron (μ_e) and hole mobility (μ_h) and the unfavorable morphology [1,2]. Regioregular poly(3-hexylthiophene) (P3HT) and [6,6]-phenyl C61-butyric acid methyl ester (PCBM) blend is one of the most promising candidates for realizing high power conversion efficiency (PCE) because P3HT possesses some unique properties over other polymers including its high self-organization capability [3,4], high hole mobility, and extended absorption in the red region of the electromagnetic

* Corresponding authors. Address: Research Center for Applied Sciences, Academia Sinica, Taipei, Taiwan. Tel.: + 886 2 27898000(x)70; fax: +886 2 27826680 (C.-W. Chu), tel.: +886 2 23660739; fax: +886 2 23623040 (K.-C. Ho).
E-mail addresses: gchu@gate.sinica.edu.tw (C.-W. Chu), kcho@ntu.edu.tw (K.-C. Ho).

1566-1199/$ - see front matter © 2008 Elsevier B.V. All rights reserved.
doi:10.1016/j.orgel.2008.09.007

spectrum. Various independent approaches have been demonstrated to improve the PCE of blends consisted P3HT and PCBM. These approaches include thermal annealing [5], post-fabrication annealing at high temperature [6], and slow film growth by controlling the solvent evaporation rate of the active layer which resulted in the reduced series resistance and improved optical absorption of the devices. Subsequent annealing of the PV cells at a high temperature promotes the aggregation of PCBM which forms bi-continuous pathways in the entire active layer with the ordered P3HT phase and enhances efficient charge separation and transport. The slow solvent evaporation speed facilitates the growth of a highly crystalline film, interchain interactions become stronger and thus improve the electroconductivities, significantly [7]. These efficient enhancements are based on the unique chemical structure of P3HT. It crystallizes along its moderately long alkyl group at the 3-position and forms a more ordered structure leading to higher charge mobilities. Subsequently, an entirely positive effect in terms of solar cell efficiency has been reported due the smaller μ_h compared with μ_e in the blend in generally.

Recently, a group of polymers that works well in solar cells is an alternating copolymer based on fluorene. Polyfluorene copolymers are well known for their high charge carrier mobility, good processability, and high absorption coefficients. The physical properties of polyfluorene derivatives can be easily tuned througth the design of various alternating copolymers. Currently, PCE approaching 3.5–5.5% have been reported by several groups for organic PV devices based on blend films of polyfluorene copolymers and PCBM [8–10]. These results indicate that the PV cells based on polyfluorene copolymers are good candidates for conversion solar energy into electricity. However, the annealing and slow growth effects on the polymer based on fluorene copolymer is still not clear. The fluorene-bithiophene copolymer, poly[9,9'-dioctyl-fluorene-co-bithiophene] (F8T2) reveals good hole transporting properties [11] and excellent thermotropic liquid crystallinity [12–15]. It has also well been explored in the area of organic field-effect transistors, with good hole transporting properties [16]. On the basis of the result, it can be expected that the charge transport in F8T2:PCBM is strongly balanced. Therefore, it appears to be one of the most promising candidates among the conjugated polymers for high efficiency polymer solar cell. In this manuscript, we fabricate PV devices based on F8T2 and PCBM. We demonstrate the annealing effect on F8T2:PCBM devices through the nanoscale morphology aspect and clarify how it influences the associated PV performance.

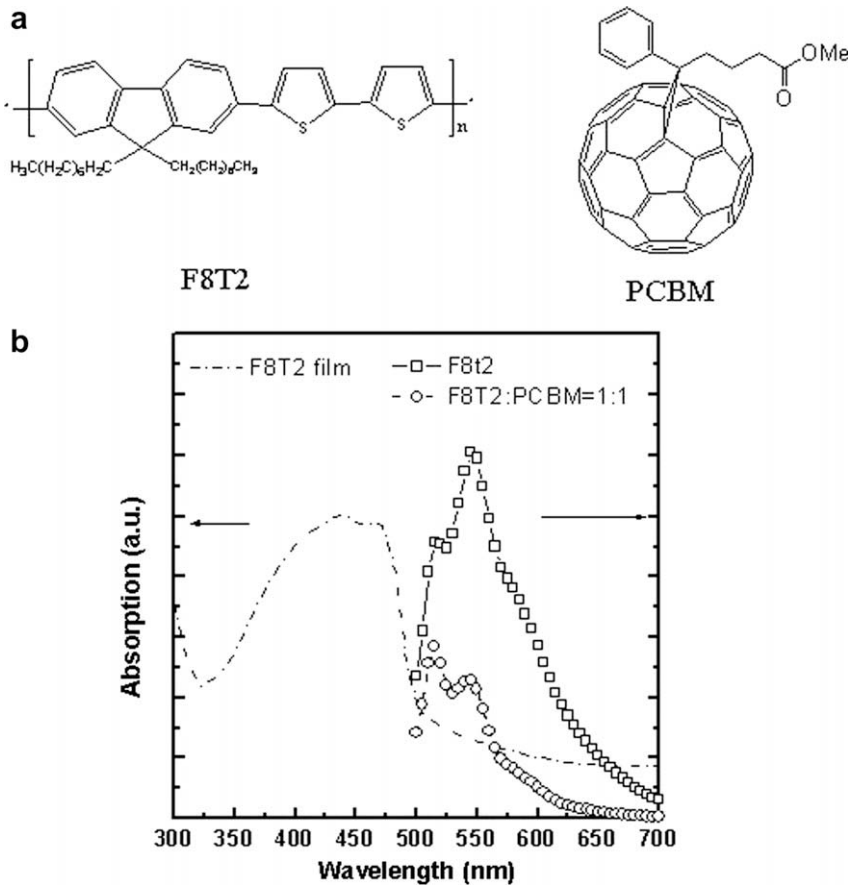

Fig. 1. (a) Chemical structure of F8T2, PCBM (b) absorption and photoluminescence spectra of pristine F8T2 and blend.

2. Experimental

The polymer PV cells in this study consists of a layer of F8T2:PCBM blend thin film sandwiched between transparent anode indium tin oxide (ITO) and metal cathode. Before device fabrication, the ITO glasses ($1.5 \times 1.5\ cm^2$) were ultrasonically cleaned in detergent, de-ionized water, acetone and isopropyl alcohol before the deposition. After routine solvent cleaning, the substrates were treated with UV ozone for 15 min. Then a modified ITO surface was obtained by spin-coating a layer of poly(ethylene dioxythiophene): polystyrenesulfonate (PEDOT:PSS) (~30 nm). Subsequently, the active layer of F8T2:PCBM (1:1 w/w) was spin coated from 1,2,4-trichlorobenzene (TCB) on the PEDOT:PSS modified ITO surface. Finally, 30 and 100 nm thick calcium and aluminium were thermally evaporated under vacuum at a pressure below 6×10^{-6} Torr through a shadow mask. The active area of the device was 0.12 cm^2.

Heavily doped p-type silicon (p^+-Si) wafer and a 300 nm thermally oxidized SiO_2 film were used as the gate and dielectric for the F8T2-based field-effect transistors (FETs). The substrates were cut to 1.5 cm × 1.5 cm in size through mechanical scribing. Prior to the deposition, the substrates were cleaned by acetone and isopropanol in an ultrasonic bath followed by UV–ozone cleaning for 15 min. The semiconductor layer F8T2 was prepared by spin-coating a solution of F8T2 (2 wt%) in TCB at 2500 rpm and with a thickness of around 110–130 nm. The F8T2 film was baked at different annealing temperature 70–250 °C for 30 min to remove the residual solvent. Finally, the 50 nm thick gold film was thermally evaporated onto the F8T2 film through a shadow mask to form the source/drain electrodes.

The solar cell testing was done inside a glove box under simulated AM 1.5 G irradiation (100 W/cm^2) using a Xenon lamp based solar simulator (Thermal Oriel 1000 W). The electrical measurements of the F8T2 based FETs were also performed at room temperature in a nitrogen environment inside a glove box by using HP 4156C. The absorption and photoluminescence (PL) spectra were obtained from Jasco-V-670 UV–visible spectrophotometer and Hitachi F-4500, respectively. Surface morphology and cross sections of thin films images were obtained using atomic force microscopy (AFM, Digital instrument NS 3a controller with D3100 stage) and scanning electron microscopy (SEM, Hitachi S-4700), respectively. X-ray diffraction (XRD) studies were performed by Philips X'Pert/MPD. Fluorescence lifetime signal was measured by the confocal laser scanning microscope (FV300, Olympus Corporation Inc.) with a configuration of PCI-board for time-correlated single photon counting (TimeHarp 200, PicoQuant GmbH) combined a detector of single photon avalanche diode (PDM series, PicoQuant GmbH). Excitation light source was 470 nm of pulse diode laser (LDH-P-C-470, PicoQuant GmbH) and acquisition time for each lifetime signal was 5 s.

3. Results and discussion

Fig. 1a shows the chemical structure of F8T2 and PCBM. The UV-visible absorption and PL emission spectra of pristine F8T2 and their blend films with PCBM are shown in Fig. 1b. The F8T2 film absorption peak is at 460 nm with a shoulder at 490 nm. The onset of the absorption occurred at 520 nm, from which the band gap was estimated to be approximately 2.4 eV. Based on cyclic voltamperometry measurements reported previously, the highest occupied molecular orbital (HOMO) level and lowest unoccupied molecular orbital (LUMO) of the polymer can be estimated at the onset point [17]. Therefore, the HOMO and LUMO levels are estimated to be 5.5 and 3.1 eV, respectively. It can be seen the band gap offset between the LUMOs of donor and acceptor is enough for electrons to be driven forward from the energy level diagram. The solid-state photoluminescence (PL) of the polymer lies near the green region with a maximum of emission at 545 nm with a vibrotic feature at 515 and 585 nm. The PL emission is significantly quenched by the addition of 50 wt% PCBM. This highly efficient photoluminescence quenching is the consequence of ultrafast photoinduced charge transfer from the polymer to PCBM.

Side view cross-sections of the films for annealing at 100 and 250 °C are shown in Fig. 2. The nanodomains are embedded within the F8T2:PCBM films. The nanodomains

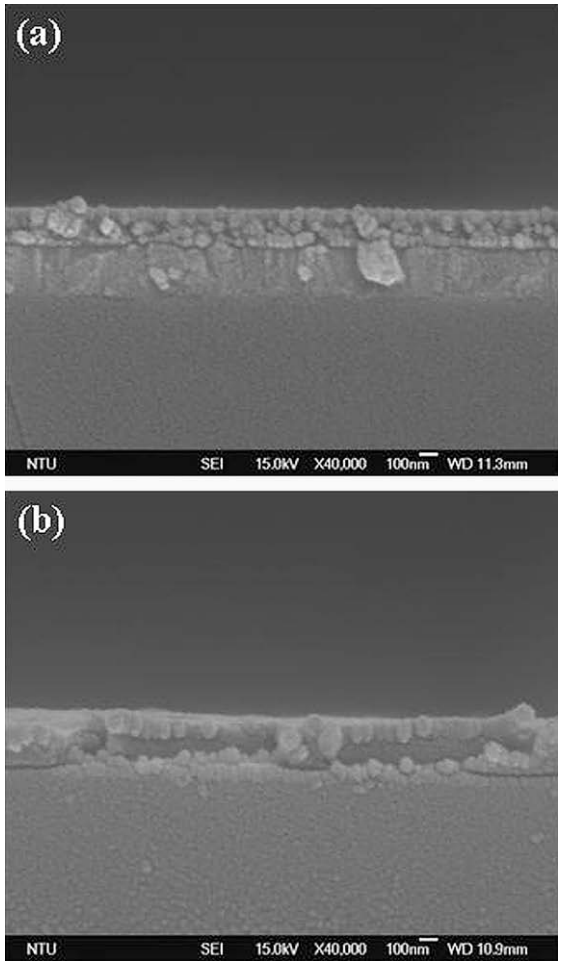

Fig. 2. SEM side views of F8T2:PCBM blend films cast from TCB annealed at (a) 100 °C (b) 250 °C.

under different annealing temperatures with diameters increased from 30–40 (100 °C) to 70–80 nm (250 °C) are assigned to the F8T2 with a coil structure formed by several polymer chains. This means the F8T2 polymer chains tend to crystallize after annealing at high temperature. The nanodomains are dispersed within the film annealed at 100 °C. Therefore, the F8T2 nanodomains and PCBM clusters are well-mixed which can achieve bi-continuous pathways in the entire layer for efficient charge separation and transport. However in the case of film annealed at 250 °C, much larger PCBM clusters can be seen. The PCBM clusters are surrounded by the polymer nanoparticles. It is expected that much of the photoexcitations will lead to recombine within the surrounding F8T2 layer. A similar result was also found for the blends based on poly[2-methoxy-5-(3,7-dimethyloctyloxy)]-1,4-phenylenevinylene (MDMO-PPV) and PCBM [18,19]. The reorganization of the F8T2 nanodomains under different annealing temperatures can be further confirmed by the observation of the surface morphology. Fig. 3 presents the AFM images for the as-cast film and the ones with thermal annealing. For the as-cast film, the surface is very smooth with a root mean square (RMS) roughness of 0.55 nm. However after undergoing thermal treatment at 130, 190 and 250 °C for 30 min, the RMS roughness increased to 0.91, 1.98 and 6.73 nm. The film without thermal annealing reveals an uniform and featureless morphology. With increasing the annealing temperature, the chain-like morphology running across the surfaces forms gradually. The features are the domains of pristine F8T2 crystallites originated from the highly tight stack of several polymer chains. For the case of annealing at 250 °C, the formation of lamella-like crystallites can be observed. The crystallites are similar to those of P3HT with the *a*-axis orientation (backbone parallel and side-chains perpendicular to the substrate) [20].

Fig. 4 shows the UV–vis and PL emission spectra under various annealing temperatures. The films annealed at the temperatures higher than 130 °C show an increase and red-shift in the UV–vis absorption. Such shifts have been observed for conjugated polymers with a strong interchain interaction [7]. The thermal annealing process enables spatial rearrangement of the polymer chains leading to a tight stacking and a strong interchain interaction. Although a higher extraction of photocurrent can be expected in the case of strong absorption. PL emission spectra also show an increase after thermal annealing. That means the photo-induced charge tends to recombine before transporting to the electrodes. This can be well explained by the SEM cross sectional images as shown in Fig. 2. The F8T2 nanodomains are dispersed in the whole film annealed at 100 °C which forms percolated pathway for electrons and holes to transport. However in the case of blend annealed at higher temperatures, the PCBM clusters are surrounded by the F8T2 nanodomains offering an inappropriate morphology for charge transport. Therefore, most of the photogenerated holes simply recombine with electrons which transport through the polymer-rich matrix phase leading to a higher emission. XRD shows that structural changes occur due to high temperature annealing process. An increase in crystallinity of F8T2 can be seen clearly in

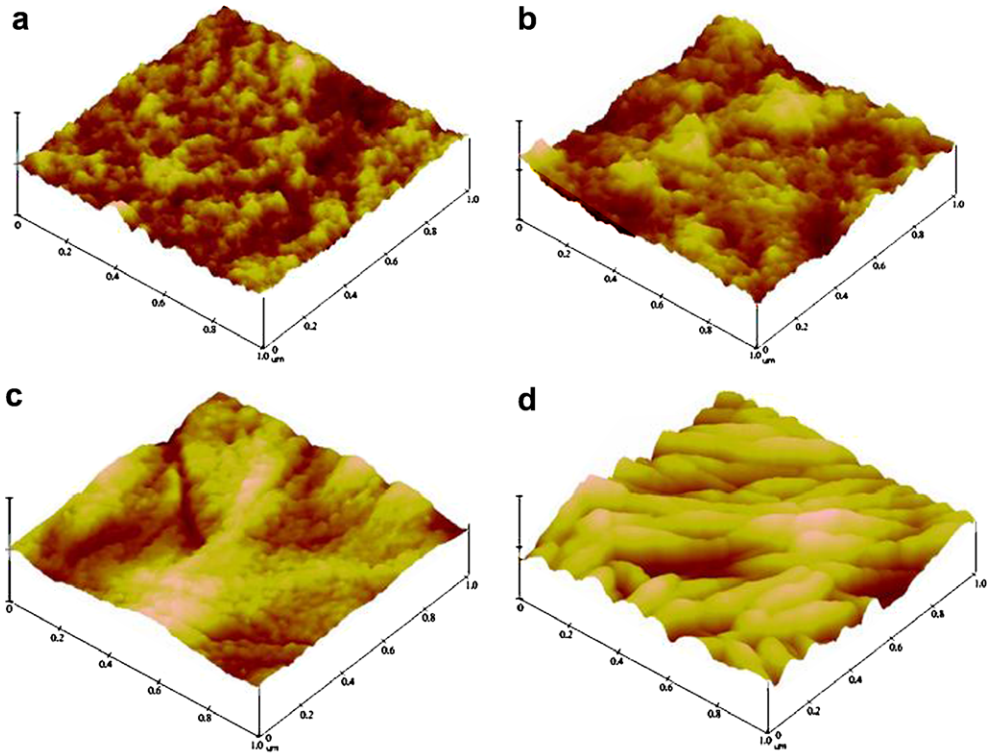

Fig. 3. AFM images of the blending films in various annealing temperature (a) as-cast film (b) 130 °C (C) 190 °C (d) 250 °C.

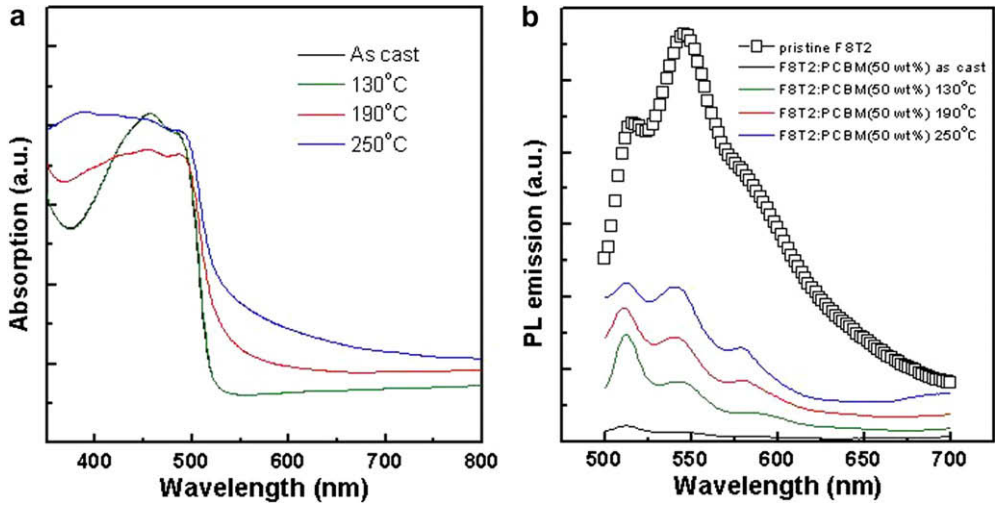

Fig. 4. (a) Absorption and (b) photoluminescence spectra of the blends annealed at different temperatures.

the results shown in Fig. 5. X-ray data show that prior to heating, the F8T2 is in a disordered state. Increased intensity is observed with increasing annealing temperature in the peak at $2\theta \approx 5.7$ which corresponds to the layering distance, d_{100} = Å, between the sheets of F8T2 chains associated with the plane perpendicular to their longitudinal axes. The features are in good agreement with the results of AFM images. This lamella structure appears due to the segregation of main chain backbones from the aggregated alkyl side chains.

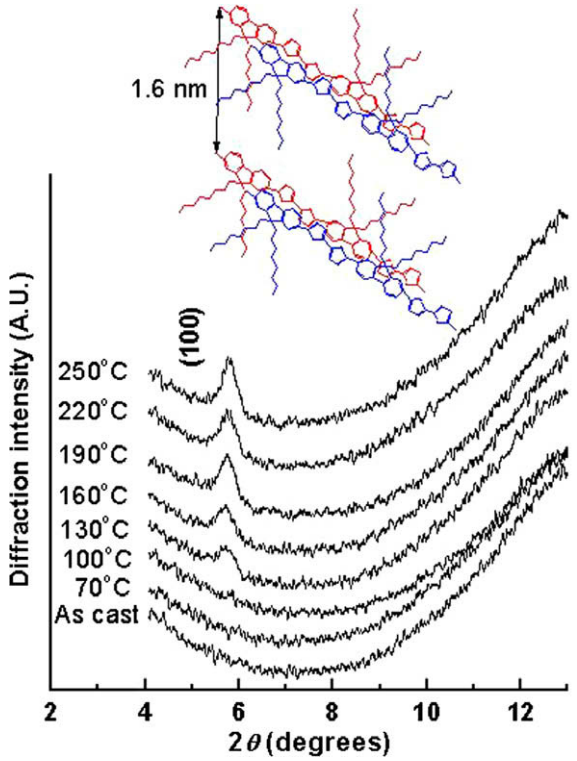

Fig. 5. XRD spectra of F8T2:PCBM films annealed at different temperatures.

Additional evidence supporting the dependence of the crystallinity of F8T2 on the annealing temperature is provided by the observation of charge transport from field effect transistors (FETs) made with F8T2. Fig. 6 shows transfer characteristic of F8T2-based FETs at different annealing temperatures. The performance of F8T2 FETs is increased with rising up the annealing temperature. The improvement of device performance is attributed to the degree of F8T2 film crystallization which is coincident with above results. When annealing temperature is at 250 °C, the corresponding devices exhibit highest hole field effect mobility, 2.7×10^{-4} cm^2/Vsec, depicting superior performance in p-channel conduction among the various annealing temperature conditions.

In order to get more careful investigation of the photophysics in the F8T2:PCBM systems, we perform the time-resolved PL to see the exciton decay as a function of annealing temperature as shown in Fig. 7. It is found the PL life time (1.87 ns) for the blend without thermal treatment is shorter than that of the pristine F8T2 thin film (3.83 ns), indicating that the charge separation occurs at the interfaces between F8T2 and PCBM by providing a new non-radiative process for photogenerated excitons. However, the exciton life time increases with increasing the annealing temperature. This indicates the thermal process results in an unfavorable morphology. The unfavorable morphology reduces the interface between F8T2 and PCBM whish is in good agreement with the SEM results as shown in Fig. 2 in the text. As the annealing temperatures increased from 70 to 250 °C, the poor morphology leads to a non-efficient charge separation and the exciton life time increases from 1.91 to 2.84 ns.

The current-voltage characteristics under illumination for PV devices that have undergone various thermal annealing are shown in Fig. 8 and the device parameters (PCE, V_{OC}, J_{SC}, FF) are summarized in Table 1. Although the FET characteristics have shown the formation of more

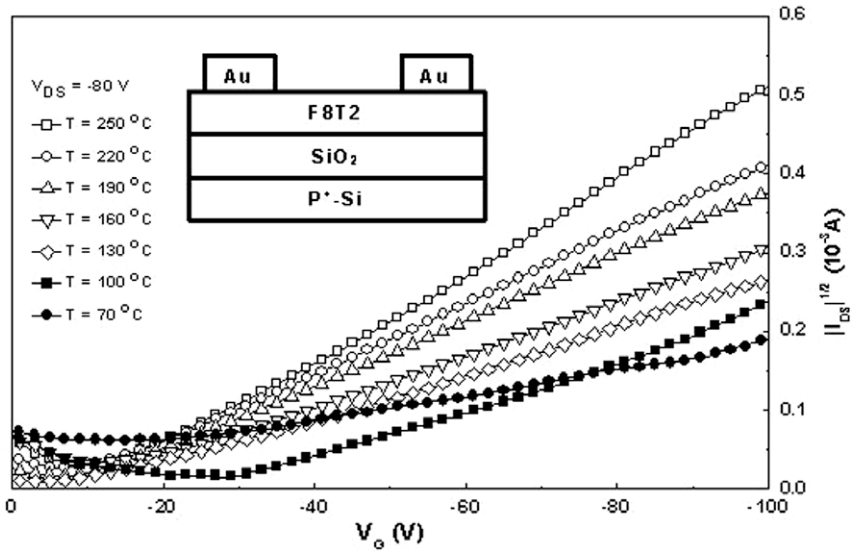

Fig. 6. Transfer characteristic of F8T2 based FETs at different annealing temperatures when drain to source voltage (V_{DS}) is −80 V. The inset is the schematic configuration of F8T2 FETs.

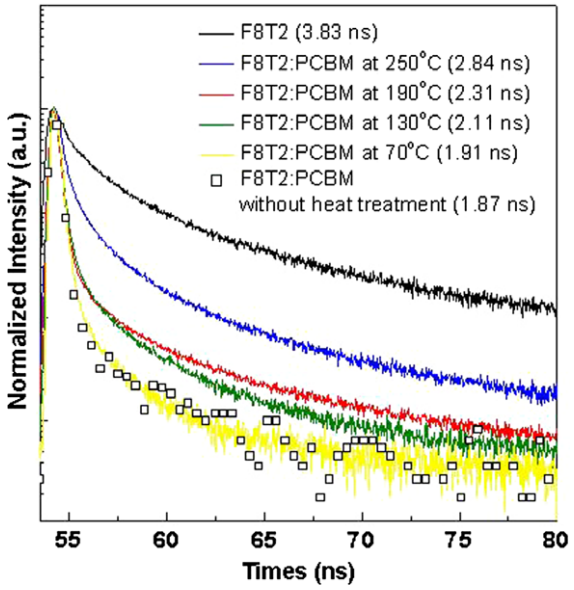

Fig. 7. Photoluminescence lifetime decay of the F8T2 and the blends annealed at various temperatures.

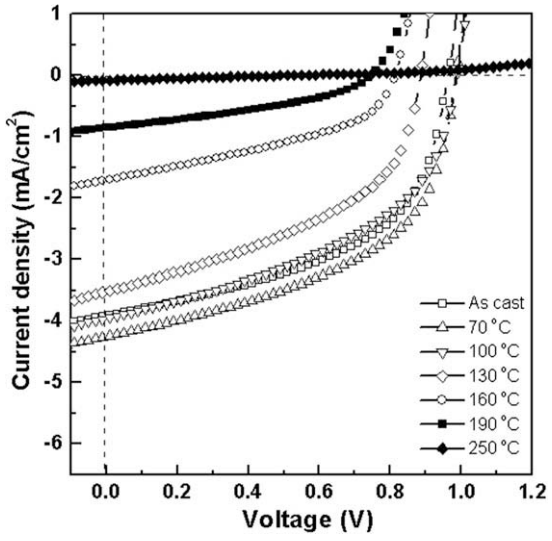

Fig. 8. *J–V* characteristics under illumination for PV devices based on F8T2:PCBM (1:1) with different annealing temperatures.

ordered structures in the blend by thermal treatment, thereby increasing the charge mobility, the unfavorable morphologies are also formed by the annealing process which leads to phase separation and charge recombination as shown in the SEM cross-sectional images. As a result of the influence by the two factors, it can be observed the photocurrent show an increase first and then a dramatic decrease while annealing temperature is higher than 130 °C. It is worthy to mention the temperature at which the values of J_{SC} and V_{OC} drop dramatically is the temperature that crystallization takes place. This means the performance of the PV devices is largely dominated by a

Table 1
Short-circuit current (J_{SC}), open circuit-voltage (V_{OC}), fill factor (FF) and power conversion efficiency (PCE) as a function of annealing temperature for the PV devices based on F8T2:PCBM with PCBM concentration equal to 50 wt%.

Annealing temp (°C)	J_{sc} (mA/cm^2)	V_{oc} (V)	FF (%)	PEC (%)
As-cast	3.91	0.97	51.4	1.95
70	4.24	0.99	50.8	2.13
100	3.94	0.99	46.7	1.82
130	3.51	0.89	45.4	1.42
160	1.71	0.82	40.5	0.57
190	0.85	0.75	37.0	0.23
250	0.08	0.48	22.0	0.01

favorable morphology and not a higher charge mobility in the F8T2:PCBM system. This results quite differ from the case in P3HT:PCBM. Several researches have been shown independently a positive effect on solar cell performance with the thermal treatment [21–23]. The best device performance was obtained at 70 °C, and the values were J_{SC} = 4.24 mA/cm^2, V_{OC} = 0.99, FF = 0.51, and PCE = 2.14% with 50 wt% PCBM cast from TCB.

4. Conclusion

In conclusion, the F8T2:PCBM blends with thermal annealing at various temperatures leads to a tunable hole mobility. Our results demonstrate that the phase separation plays a more significant role than the one of charge mobility in terms of solar cell performance. Based on the results, too high annealing temperature is unfavorable to the performance of PV devices. Consequently, the optimal annealing temperature appears to be 70 °C and the PCE up to 2.14% can be obtained.

Acknowledgements

The authors are also grateful to the National Science Council (NSC), Taiwan, (NSC 97-2120-M-002-012 and NSC 96-2221-E-001-017-MY2) and Academia Sinica Research Program on Nanoscience and Nanotechnology for financial support.

References

[1] C. Goh, R.J. Kline, M.D. McGehee, E.N. Kadnikova, J.M.J. Frechet, Appl. Phys. Lett. 86 (2005) 122110.
[2] V.D. Mihailetchi, J.K.J. van Duren, P.W.M. Blom, J.C. Hummelen, R.A.J. Janssen, J.M. Kroon, M.T. Rispens, W.J.H. Verhees, M.M. Wienk, Adv. Funct. Mater. 13 (2003) 43.
[3] M. Campoy-Quiles, T. Ferenczi, T. Agostinelli, P.G. Etchegoin, Y. Kim, T.D. Anthopoulos, P.N. Stavrinou, D.D.C. Bradley, J. Nelson, Nat. Mater. 7 (2008) 158.
[4] V. Shrotriya, Y. Yao, G. Li, Y. Yang, Appl. Phys. Lett. 89 (2006) 063505.
[5] F. Padinger, R.S. Rittberger, N.S. Sariciftci, Adv. Funct. Mater. 13 (2003) 85.
[6] A.K. Pandey, J.M. Nunzi, H. Wang, C.C. Oey, A.B. Djurišić, M.H. Xie, Y.H. Leung, K.K.Y. Man, W.K. Chan, Org. Electron. 8 (2007) 396.
[7] G. Li, V. Shrotriya, J. Huang, Y. Yao, T. Mariarty, K. Emery, Y. Yang, Nat. Mater. 4 (2005) 864.
[8] K.G. Jespersen, F. Zhang, A. Gadisa, V. Sundström, A. Yartsev, O. Inganäs, Org. Electron. 7 (2006) 235.
[9] A. Gadisa, W. Mammo, L.M. Andersson, S. Admassie, F. Zhang, M.R. Andersson, O. Inganas, Adv. Funct. Mater. 17 (2007) 3836.
[10] E.G. Wang, L. Wang, L.F. Lan, C. Luo, W.L. Zhuang, J.B. Peng, Y. Cao, Appl. Phys. Lett. 92 (2008) 033307.
[11] J. Boucle, P. Ravirajan, J. Nelson, J. Mater. Chem. 17 (2007) 3141.
[12] J. Jo, D. Vak, Y.Y. Noh, S.S. Kim, B. Lim, D.Y. Kim, J. Mater. Chem. 18 (2008) 654.
[13] M.C. Gather, D.D.C. Bradley, Adv. Funct. Mater. 17 (2007) 479.
[14] L.R. Pattison, A. Hexemer, E.J. Kramer, S. Krishnan, P.M. Petroff, D.A. Fischer, Macromolecules 39 (2006) 2225.
[15] H. Sirringhaus, T. Kawase, R.H. Friend, T. Shimoda, M. Inbasekaran, W. Wu, E.P. Woo, Science 290 (2000) 2123.
[16] E. Lim, B.J. Jung, M. Chikamatsu, R. Azumi, Y. Yoshida, K. Yase, L.M. Do, H.K. Shim, J. Mater. Chem. 17 (2007) 1416.
[17] T. Ishwara, D.D.C. Bradley, J. Nelson, P. Ravirajan, I. Vanseveren, T. Cleij, D. Vanderzande, L. Lutsen, S. Tierney, M. Heeney, I. McCulloch, Appl. Phys. Lett. 92 (2008) 053308.
[18] H. Hoppe, N.S. Sariciftci, J. Mater. Chem. 16 (2006) 45.
[19] H. Hoppe, M. Niggemann, C. Winder, J. Kraut, R. Hiesgen, A. Hinsch, D. Meissner, N.S. Sariciftci, Adv. Funct. Mater. 14 (2004) 1005.
[20] T.A. Chen, X. Wu, R.D. Rieke, J. Am. Chem. Soc. 117 (1995) 233.
[21] Y. Kim, S.A. Choulis, J. Nelson, D.D.C. Bardley, Appl. Phys. Lett. 86 (2005) 063502.
[22] A. Zen, J. Pflaum, S. Hirschmann, W. Zhuang, F. Jaiser, U. Asawapirom, J.P. Rabe, U. Scherf, D. Neher, Adv. Funct. Mater. 14 (2004) 757.
[23] G. Li, V. Shrotriya, Y. Yao, J.S. Huang, Y. Yang, J. Mater. Chem. 17 (2007) 3126.